Volume 1
Number 2
February 2022
Pages 57–130

Energy Advances

rsc.li/energy-advances

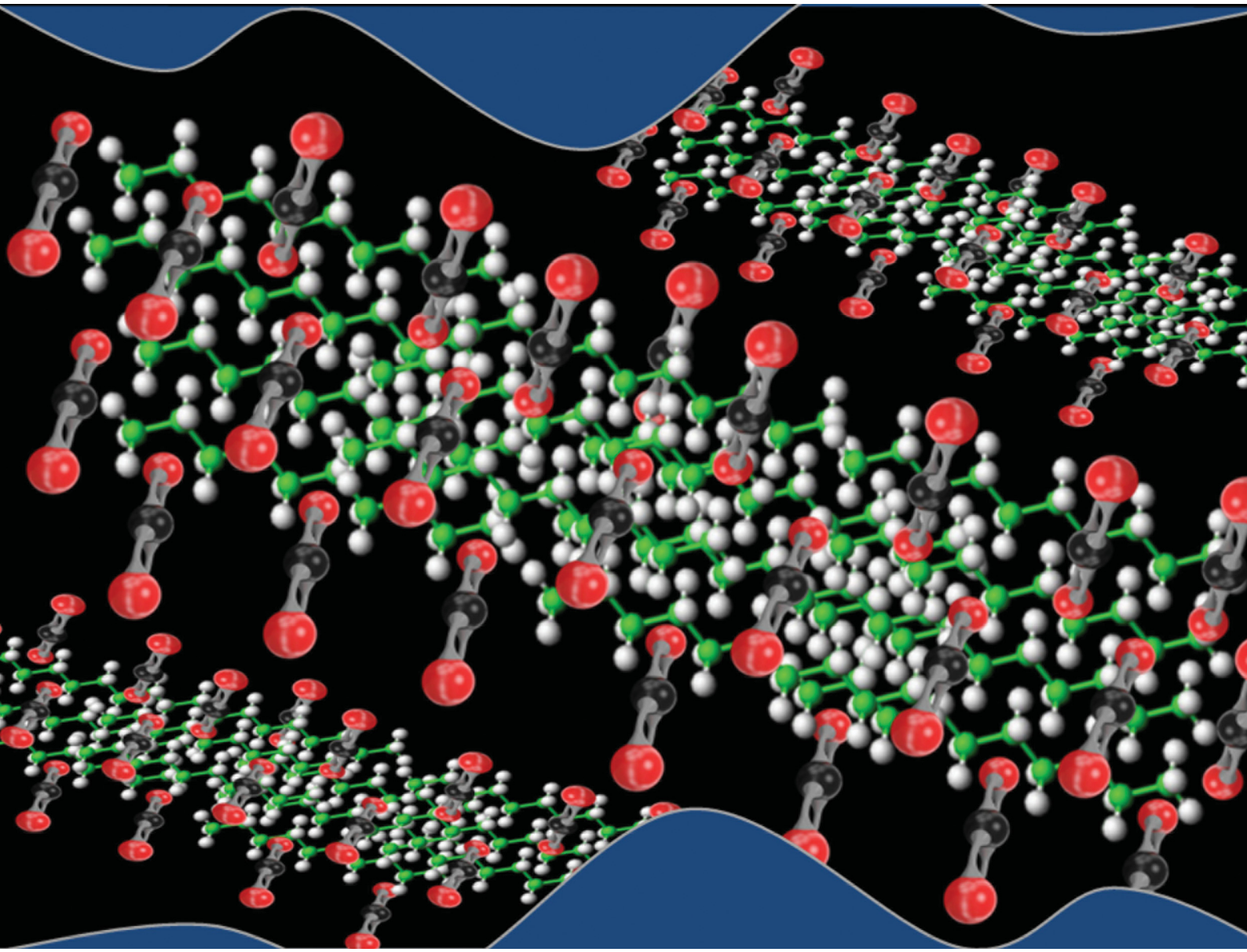

ISSN 2753-1457

ROYAL SOCIETY OF CHEMISTRY

PAPER

Konstantinos L. Stefanopoulos *et al.*
Monitoring the CO_2 enhanced oil recovery process at the nanoscale: an *in situ* neutron scattering study

Energy Advances

ROYAL SOCIETY OF CHEMISTRY

PAPER

View Article Online
View Journal | View Issue

Cite this: *Energy Adv.*, 2022, 1, 67

Monitoring the CO_2 enhanced oil recovery process at the nanoscale: an *in situ* neutron scattering study†

Konstantinos L. Stefanopoulos, *[a] Evangelos P. Favvas, [a] Georgios N. Karanikolos,[bc] Waleed Alameri,[d] Vassilios C. Kelessidis,[d] Tristan G. A. Youngs[e] and Daniel T. Bowron[e]

Received 23rd November 2021,
Accepted 12th January 2022

DOI: 10.1039/d1ya00058f

rsc.li/energy-advances

The CO_2 Enhanced Oil Recovery (CO_2-EOR) process was monitored in real time at the nanoscale by neutron scattering. This was achieved by *in situ* injection of supercritical CO_2 into a limestone sample loaded with deuterated *n*-decane. The experimental results show directly the decane displacement upon supercritical CO_2 injection. The structure of CO_2 confined in the pores has also been evaluated and compared to that in the bulk state. Finally, analysis of the neutron results shows that small mesopores have low accessibility to CO_2 suggesting that they will not be available for storage for geologic CO_2 sequestration.

Broader context

Carbon capture and storage (CCS) has been recognized as a key technology to reduce greenhouse gas emissions in an attempt to limit the effects of global climate change. Nowadays, carbon dioxide-enhanced oil recovery (CO_2-EOR) has gained global attention in light of declining oil reserves. The potential of combining CO_2-EOR technology with CCS has the benefits of enhanced oil recovery and permanent storage of an amount of injected CO_2 in the depleted reservoir. Further advancement of CO_2-EOR technology requires a better understanding of the fundamental mechanism at the nanoscale. *In situ* neutron scattering and supercritical CO_2 injection into reservoir rocks provide novel insights into the oil displacement and the structural arrangement of CO_2 molecules confined in the nanopores. Additionally, porosity is one of the parameters that determines the extent to which CO_2 will be stored during the CO_2-EOR. The fact that neutrons can detect both open and closed porosity means that the applied methodology provides also valuable information about the pore accessibility to CO_2 and, thus, the potentiality for geological sequestration.

1. Introduction

It is estimated that more than 50% of original-oil-in-place remains unrecovered after the primary and secondary phases of oil recovery.[1] Enhanced oil recovery (EOR) is applied as a tertiary recovery phase. Gas injection or miscible flooding is nowadays a widely used method in EOR. Specifically, carbon dioxide-enhanced oil recovery (CO_2-EOR) has attracted global attention in light of declining conventional oil reserves. CO_2-EOR has the major advantage of additional hydrocarbon recovery that promotes energy independence. Moreover, CO_2-EOR may play a crucial role in the reduction of the global emissions of greenhouse gases because CO_2 either remains sequestered underground in the subsurface geologic formations or is re-captured and re-injected in a subsequent EOR project.[2] Another benefit of CO_2-EOR projects is that the same site could be also used, without any additional investment, for further CO_2 sequestration after the project completion.[3] It is estimated that more than 90% of the world's oil reservoirs are potentially appropriate for CO_2-EOR, which implies that about 140 Gt CO_2 could be used and stored in this way.[4] In addition, CO_2-EOR accounts for approximately 5% of the total US crude oil production.[4] Furthermore, CO_2-EOR currently provides the largest market demand for CO_2, with the potential to generate revenue from the production of over 1000 billion barrels of oil while storing over 300 Gt CO_2 globally.[5] This means that carbon

[a] *Institute of Nanoscience & Nanotechnology, NCSR "Demokritos", 153 10 Ag. Paraskevi Attikis, Athens, Greece. E-mail: k.stefanopoulos@inn.demokritos.gr*
[b] *Department of Chemical Engineering, Khalifa University, P.O. Box 127788, Abu Dhabi, United Arab Emirates*
[c] *Research and Innovation Center on CO_2 and H_2 (RICH), Khalifa University, P.O. Box 127788, Abu Dhabi, United Arab Emirates*
[d] *Department of Petroleum Engineering, Khalifa University, P.O. Box 127788, Abu Dhabi, United Arab Emirates*
[e] *ISIS Neutron and Muon Source, STFC Rutherford Appleton Laboratory, Harwell Oxford, Didcot, OX11 0QX, UK*

† Electronic supplementary information (ESI) available. See DOI: 10.1039/d1ya00058f

capture and storage enhanced oil recovery (CCS-EOR) can be balanced with the dual objective of enhanced oil recovery whilst at the same time storing some of the injected CO_2 permanently in the depleted reservoir.[6–11] Finally, in a recent review study it was suggested that it is feasible to use CO_2-EOR to enhance shale gas recovery instead of using conventional water-based fracturing fluids. It was then concluded that the process can be applied with the objectives of drilling, fracturing and sequestration.[12]

Injected carbon dioxide alters the properties of the residual oil within the pores in order to make it mobile and extractable. CO_2 may either become miscible or remain immiscible with oil, depending on the oil properties and the reservoir temperature and pressure.[13] The most crucial parameter is the pressure at which miscibility is achieved, defined as the minimum miscibility pressure (MMP). In the case of the miscible CO_2-EOR process, the reservoir pressure is above the MMP and the higher and intermediate molecular weight reservoir oil hydrocarbons vaporize into the CO_2, whilst part of the pressurised CO_2 dissolves into the oil. This mass transfer between the oil and CO_2 allows the miscibility of the two phases without any interface; as a result, a transition miscible zone is developed with the CO_2 in the back and the oil in the front.[14] In most cases the miscible CO_2-EOR mode is preferable because it achieves higher oil recoveries compared to the immiscible methodology. On the other hand, when the reservoir pressure is below the MMP, the oil and CO_2 do not form a single phase and they are not miscible. However, CO_2 dissolves in the oil causing oil swelling and reduction in viscosity thus also resulting in oil recovery. Finally, the use of additives can enhance the oil recovery and reduce the cost by further improving the miscibility behavior of CO_2 and oil and lowering the MMP respectively.[15] From this point of view, it is important to develop an in-depth understanding of the structural properties of both the porous host and the pore-confined CO_2 during the CO_2-EOR process at the nanoscale.

Fluids when confined within nanopores have unique thermodynamic, structural and dynamic properties that vary significantly from those in the bulk phase because of the finite pore size and the fluid interaction with the pore wall.[16] In general, there are still many open questions in the study of fluids confined in nanoporous materials[17] and in spite of the large existing body of literature, a comprehensive theory is yet to be established. Elastic neutron scattering techniques such as neutron diffraction, total neutron scattering, small-angle neutron scattering (SANS) and ultra-small-angle neutron scattering (USANS) are uniquely powerful tools that allow us to investigate the microstructure of porous materials[18] as well as the location, the structure, and the phase behavior of fluids confined within their pores.[19] In addition, inelastic (or quasielastic) neutron scattering techniques are also essential tools to reveal the dynamics of fluids confined in porous materials.[20,21]

The total neutron scattering method provides unique information about the structure of disordered materials containing light elements. In general, disorder disrupts the perfect periodicity or the long-range order of crystalline materials that gives rise to Bragg scattering. Disordered materials such as liquids, polymers, glasses and porous solids exhibit only short-range order over a distance of few atoms. The correlations between the disordered structural characteristics give rise to diffuse scattering. The total neutron scattering method takes into account both Bragg scattering and diffuse scattering signals. As a result, the interference differential scattering cross section, $F(Q)$, and its inverse Fourier transform, the differential pair correlation function, $D(r)$, can be derived.[22,23] Earlier studies that combined CO_2 sorption (at various thermodynamic states) and total neutron scattering on ordered mesoporous materials (MCM-41, SBA-15, CMK-3) have revealed the structural details of pore-confined CO_2.[24–27] Surprisingly, it was also observed that during freezing SBA-15 and CMK-3 samples loaded with CO_2 below the bulk critical point, the confined CO_2 molecules did not freeze or remain liquid as expected, but escaped from the pores.[26,27] Moreover, when the total scattering data are combined with atomistic Monte Carlo simulations, detailed information concerning the accurate positions of the confined fluids within the pores can be extracted.[28,29] As these experimental methodologies move closer to addressing real world examples, the complex pore architecture of sedimentary rocks is of great importance because the microstructure and evolution of porosity plays a critical role in many geological processes including CO_2 sequestration and oil recovery. In case of shales, the neutron scattering results showed that mineralogical variations have little effect on the behavior of CO_2 within the micropores hosted in the organic matter of the shale at high thermal maturities. In addition, the results have elucidated that the confined CO_2 is in a densified state having liquid-like properties.[30,31] It is noteworthy that strong densification of confined CO_2 has also been observed in microporous carbon[32–35] and in ordered mesoporous carbon (CMK-3) samples.[27]

Complementary to total neutron scattering that measures interatomic distances, small-angle neutron scattering (SANS) and ultra-small-angle neutron scattering (USANS) probe the structures at larger length scales, varying from 1 nm to a few hundred nanometers (SANS) and up to about 10 μm (USANS). (U)SANS is a non-invasive technique and provides information about the pore geometry and topology, the texture of the matrix-pore interface (smooth or rough), the total porosity, the pore size distribution and the specific surface area.[36–39] The same properties can also be explored by the traditional gas sorption and mercury porosimetry methods but their limitation is that they can only probe the accessible (open) pores. On the other hand, neutrons have also the ability to ''see'' the pores that are inaccessible to the invading fluid (closed pores). This can be attained by conducting contrast-matching SANS (CM-SANS). The technique is applied by carrying out SANS on dry samples where the signal arises from all the pores including accessible (open) and inaccessible (closed) pores. Then the scattering from open pores can be eliminated by saturating the porous material with a contrast matching mixture of a hydrogenous and deuterated solvent (for example H_2O/D_2O).[40] As a result, any scattering signal yields information only about the closed

pores.[41–46] Melnichenko and coworkers suggested an alternative method of achieving contrast matching in porous media by using non-adsorbing or weakly-adsorbing supercritical fluids or pressurised gases, such as CO_2 or methane on carbonates,[47] coal,[48–52] and shale.[52–54] It is worth mentioning that the neutron capability of differentiating between open and closed porosity is of great importance for the study of underground CO_2 sequestration in sedimentary formations. For instance, in the case of shale, neutron scattering measurements suggest that oil recovery would be unlikely to displace petroleum from some of the smaller mesopores and all of the micropores because they are effectively closed to CO_2. This finding is also interesting because it suggests that during anthropogenic CO_2 sequestration, the vast number of micropores in shale will be unavailable for storage because they are all inaccessible or closed to CO_2.[30,31]

In the present study, we attempt to establish a new methodology to monitor the CO_2-EOR process in real time by neutron scattering. In particular, the oil recovery process is explored at the nanoscale by utilising total neutron scattering by *in situ* injection of supercritical CO_2 fluid into a limestone sample loaded with deuterated *n*-decane. In addition, the structure of confined supercritical CO_2 and the pore accessibility to CO_2 have also been evaluated. It is worth mentioning that NIMROD was the neutron instrument of choice because its wide *Q*-range capabilities mean that it also probes a significant part of SANS region. From this point of view, a combination of total neutron scattering and SANS techniques have been carried out simultaneously.

2. Experimental methods and materials

a. Sample preparation

All the core samples were Indiana limestones composed mainly of calcium carbonate ($CaCO_3$) (97.30%), $MgCO_3$ (0.40%), Al_2O_3 (0.50%) and SiO_2 (1.70%). The average porosity is 18% and the average permeability is about 150 mD.

The provided dry core samples had dimensions of 4 cm in length and 38 mm in diameter. The cores were then cut to subcores with 4 cm length and a thickness of 3.9 mm by using a BRUEHLER precision cutter (Fig. S1f in ESI†). The subcores were sized to these dimensions in order to fit tightly into a high-pressure sample container (Fig. S1c and S2 in ESI†) to minimise any obscure scattering from the non-adsorbed supercritical CO_2. One of the subcores was loaded with deuterated *n*-decane as follows: it was placed in an atmospheric oven and left overnight at 250 °C. As soon as it was removed from the oven it was then placed in a vessel containing deuterated *n*-decane. The sample remained there for 12 hours and after removal it was allowed to dry in a humidifier with 30% relative humidity.

b. Neutron scattering experiment

The total neutron scattering experiment was conducted on the NIMROD instrument located at Target Station 2 of the ISIS Neutron and Muon Source, STFC Rutherford Appleton Laboratory, Oxfordshire, UK (Fig. S1a in ESI†). One of the main advantages of this particular instrument is that it delivers an extended *Q*-range that also covers a significant regime of SANS. Specifically, NIMROD's *Q*-range varies between 0.02 and 50 $Å^{-1}$; where *Q* is the magnitude of the scattering vector defined as $Q = 4\pi \sin\theta/\lambda$, where 2θ is the scattering angle and λ is the neutron wavelength. This corresponds to the ability to probe real space structures on length scales ranging from 0.1 Å to 300 Å, and explore complex systems such as disordered materials (liquids, confined fluids, glasses, porous solids *etc.*) with unprecedented detail. In addition, NIMROD delivers high neutron flux and low background that are necessary characteristics to facilitate the measurement of weak signals arising from diffuse scattering with good statistics. Importantly, NIMROD allows for the integration of advanced sample environment including gas handling equipment, cryostats, furnaces and high-pressure sample containers that are required for *in situ* monitoring of sample processes. The instrument is thus ideal for investigation of nanoscale phenomena such as sorption, catalysis, and operando charging–discharging of batteries based on nanostructured substrates.[23,55]

In the present study we used a high-pressure (up to 1 kbar), custom-made null scattering $Ti_{0.676}Zr_{0.324}$ cell as a sample container (Fig. S1c and S2 in ESI†). The sample preparation took place in the chemistry laboratory close to NIMROD (Fig. S1e in ESI†). The high-pressure sample container (with temperature control) was then mounted on a candlestick connected to a gas handling manifold equipped with a pressure intensifier (to get high-pressure supercritical CO_2), a pressure transducer (0–300 bar), a relief valve (200 bar), a turbo pump vacuum system, and gas and vacuum connections (Fig. S1b in ESI†). The gas line was then connected to a high-purity CO_2 cylinder (99.9996%) system with the aid of a reducer. Finally the whole stick was inserted in the neutron beam under vacuum (Fig. S1d in ESI†). The neutron beam width was 1 cm and the height was 3 cm. The neutron measurements were conducted at 393 K. The selected temperature is the upper limit that has been observed as favourable for miscibility to proceed.

As a first step a dry subcore with empty pores (under vacuum) was measured and then loaded with supercritical CO_2. The limestone samples were pressurised with purified supercritical CO_2 up to 180 bar. The neutron scattering profiles were collected after equilibrium at each CO_2 pressure point.

As a next step, the subcore loaded with deuterated *n*-decane was measured at 293 K for 2 hours; it is worth mentioning that the filled subcore was measured after 24 hours in order to equilibrate and to be sure that decane has penetrated even the finest pores. Then it was heated at 393 K and another neutron run took place for 2 hours (no differences were observed). After, the oil recovery process was measured by *in situ* injection of supercritical CO_2 at 164 bar for 4 hours. Finally, another neutron run was carried out for 2 hours and a partial decane displacement was clearly observed. Measurements of bulk supercritical CO_2 (393 K) and deuterated *n*-decane (293 K) were also conducted for direct comparison to the confined phases.

The raw neutron scattering data were then corrected for instrument and sample container backgrounds, absorption, multiple and inelastic scattering and they were also normalized to a vanadium-niobium standard using the Gudrun analysis routines.[56] The Facility's Gudrun software has also been used to deduce the total structure factors and the correlation functions from the inverse Fourier transforms of the structure factors.

3. Results and discussion

a. *In situ* neutron scattering and CO_2 injection in limestone with empty pores

Fig. 1 illustrates the neutron scattering curves from the dry limestone sample (with empty pores) under vacuum at 393 K and after *in situ* injection with supercritical CO_2 at 130 bar and 180 bar respectively. As a first remark, in the SANS region ($0.012 < Q$ (Å^{-1}) < 0.07), the scattering profiles do not vary significantly with CO_2 pressure. Simulations have shown that for polydisperse porous materials, such as natural porous systems, an appropriate empirical relationship relating the scattering vector, Q, with the pore radius, r, (assuming spherical pores) is $r \sim 2.5/Q$.[57] As a result, the SANS region corresponds to pore radii $208 < r$ (Å) < 36 (these pores are mesopores; the mesopores are defined as a class of pores with pore radii in the range between 10 and 250 Å). However, the SANS signal arising from the dry limestone specimen is slightly stronger compared to that of the limestone upon supercritical CO_2 loading at both pressures (Fig. 1). This means that the supercritical CO_2 injection reduces the scattering contrast and, thus, the scattered intensity between the limestone matrix and the carbon dioxide. This reduction in the intensity is caused by the sorption of the gas on the pore surfaces and the density increase of supercritical CO_2 with pressure.

In addition, this particular SANS region shows a linear region for the dry limestone specimen on a log–log scale (Fig. 1). The gradient of this linear regime is −3.2. This power law scattering is characteristic of a very rough (or fractally rough) pore-solid matrix interface. The result is in agreement with previous (U)SANS measurements on carbonate specimens where the gradient varies between −3.1 and −3.7.[47] Again, this linear regime is dominated by the scattering from pores of linear dimensions in a length scale 36–208 Å. In addition, the slope does not vary significantly upon pressurized supercritical CO_2 injection, suggesting no structural changes of the solid matrix caused by possible damage to the pore morphology. This is further verified from the fact that no hysteresis was observed after the removal of the supercritical fluid from the pore matrix; the scattered intensity returns to the initial profile of the dry sample under vacuum (not shown in Fig. 1).

At high Q scattering, however, ($Q > 0.07$ Å^{-1}) the opposite behavior is observed, *i.e.* the injection of supercritical carbon dioxide in pores smaller than 36 Å increases the scattered intensity significantly (Fig. 1). The increase in the intensity is mainly caused by the density fluctuations in supercritical CO_2 in the high-Q region. Finally, for $Q > 1.62$ Å^{-1} the Bragg reflections of the limestone sample are clearly visible where most of them originate from calcium carbonate ($CaCO_3$) which is to be expected (see also ESI,† Fig. S6, inset).

As mentioned in the introduction, one of the advantages of scattering methods is the neutron capability of differentiating accessible (open) and inaccessible (closed) porosity. This information is of great importance for the global requirement to reduce CO_2 emissions during the injection to the oil reservoirs for CO_2-EOR. The reason is that an amount of the injected CO_2 could be securely stored in the reservoir resulting in a reduction of the greenhouse emissions. Additionally, closed pores may play a crucial role in the oil recovery because they may also contain hydrocarbons and, thus, the efficiency of the CO_2-EOR process could also depend on the extent to which they can be accessed. Melnichenko and co-workers utilised the neutron contrast-matching method to determine the volume fraction of accessible pores in natural porous systems by *in situ* injecting pressurised greenhouse gases such as CO_2 and CH_4. Specifically, by measuring the neutron scattering curves as a function of fluid pressure, when the contrast matching pressure (or the zero average contrast, ZAC) is attained, the remaining scattering signal simply suggests the presence of pores inaccessible to fluid. The ZAC condition, however, cannot always be achieved because in some cases (depending on the mineral composition and the fluid selection), very high fluid pressures in the order of kilobars may be required. Alternatively, a methodology has been developed[47] for the calculation of accessible and inaccessible pores without the requirement of the achievement of ZAC (see ESI,† Section 4). The inset in Fig. 1 presents the evaluated accessible pore fraction as a function of the pore radius. The result suggests that the accessibility of large mesopores (with pore radius 150–200 Å) is much larger (~80%) compared to that of small mesopores. For instance, the accessibility of pores with radii 40 Å drops down to about 30% (Fig. 1, inset). The result strongly suggests that the small mesopores are unlikely sites for underground CO_2 sequestration. This finding is also in agreement with recent neutron experiments in shale that also showed that some of the smaller mesopores and all of the micropores are effectively closed to CO_2.[30,31]

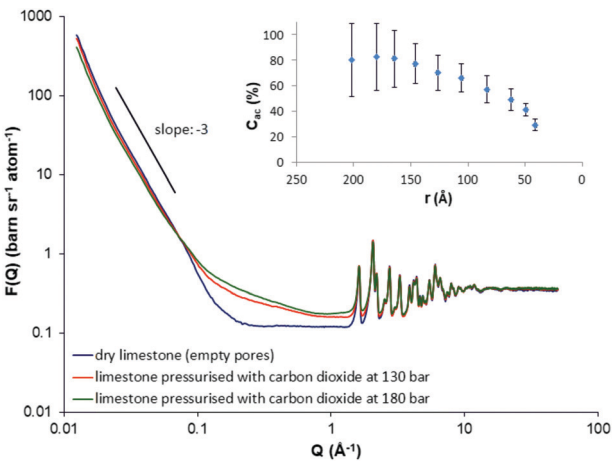

Fig. 1 Neutron scattering profiles of limestone sample during pressurisation with supercritical CO_2 at 393 K. Inset: The calculated volume fraction of accessible pores (with the error bars) as a function of pore radius.

b. Structural profile of pore-confined CO_2

The total neutron scattering profiles can also reveal the structural details of bulk liquids, despite the lack of long-range order, by evaluating the total structure factor comprising the intermolecular structure peak (representing the most probable distance between nearest-neighbour molecules) and the intramolecular oscillations (within the molecule) arising at higher Q values. In addition, when a fluid is confined in the pores, the structure factor is the superposition of the matrix–matrix (limestone), the fluid–fluid (CO_2), and also of the matrix–fluid interactions (between the limestone matrix and the CO_2). The matrix–fluid contribution is usually referred as cross-correlation term originating mainly from the interactions of confined CO_2 molecules with the pore walls. The matrix–matrix contribution can be easily subtracted from the experimental data of the dry limestone sample with empty pores. Finally, the experimental data are reduced to the ''total structure factor'' of confined CO_2 comprised of the fluid–fluid interaction (corresponding to the structure factor of the bulk CO_2) and the cross-correlation term (containing the confinement effects). The evaluated total structure factor of pore-confined CO_2 is proportional to the absolutely calibrated differential cross section obtained by standard methods (see ref. 24 and 58 for quantification details of the total structure factor evaluation).

Following the procedure described above, Fig. 2a shows the calculated total scattering structure factor for the confined supercritical CO_2 in limestone rock at 393 K and 180 bar (confined SC2). In addition, the structure factor for the bulk supercritical CO_2 (SC2) at the same thermodynamic state is also shown for comparison (see also ESI,† Fig. S3). It can be seen that both structure factors (bulk and confined) have some similarities. For instance, a strong SANS signal is also pronounced in the case of confined supercritical CO_2. This finding suggests that the carbon dioxide molecules form clusters even within the pore matrix of the limestone. Another interesting feature is that the confined phase presents also an intermolecular structure peak, however, slightly broadened and shifted to a larger Q value (1.50 $Å^{-1}$) compared to the bulk phase (1.39 $Å^{-1}$). The result suggests that pore-confined CO_2 is also in a densified supercritical state having higher density compared to that of the bulk one (Fig. 2b). The result also suggests that the presence of the confining matrix impacts the orientational freedom of the near surface CO_2 molecules, and thus affects a certain proportion of the confined fluid. Finally, it is noteworthy that the observed periodic oscillations at high Qs are also clearly visible for the confined phase implying that the confined supercritical CO_2 is characterised by a short-range order too (Fig. 2a). The clustering and the short-range order of the CO_2 molecules can be interpreted in terms of the relatively large accessibility of large mesopores (Fig. 1, inset) and the reasonable sample porosity (about 18%) and permeability (about 150 mD). In contrast, when CO_2 was confined in the pores of Marcellus shale, only one intramolecular peak was visible suggesting small CO_2 sorption because of the low sample porosity (about 2.5%) and the small pore accessible volume fraction.[30] Moreover, the lack of short-range order in the shale samples was also attributed to the physical inability of CO_2 to pack perfectly within the pores of the shale matrix.

c. *In situ* neutron scattering and CO_2 injection in limestone filled with *n*-decane-D22: monitoring the CO_2-EOR at the nanoscale

Fig. 3 (blue curve) shows the neutron scattering curve from the limestone filled with decane during the *in situ* CO_2-EOR process at 393 K (*n*-decane-D22 was the preferred choice in order to minimise the incoherent background scattering from hydrogen). The most striking evidence of the decane presence within the limestone is the clearly observed peak at 1.27 $Å^{-1}$ (see also ESI,† Section 5, for a comparison of the scattering curves between the empty limestone and the limestone filled with decane). As a next step, supercritical CO_2 was injected *in situ* at the sample at a pressure close to the MMP (P = 164 bar) for 4 hours (see ESI,† Section 6). During the CO_2 injection, the scattering curve changes dramatically resulting in the disappearance of the decane peak (Fig. 3, red curve). According to the theory of CO_2-EOR, a part of the pressurised CO_2 dissolves into the oil resulting in oil swelling. From this point of view, the absence of the short-range decane ordering can be attributed to the CO_2 dissolution combined with the dynamic displacement of decane. After termination of the supercritical CO_2 injection, a decrease in the decane peak is clearly observed suggesting that an amount of decane has been removed (Fig. 3, green

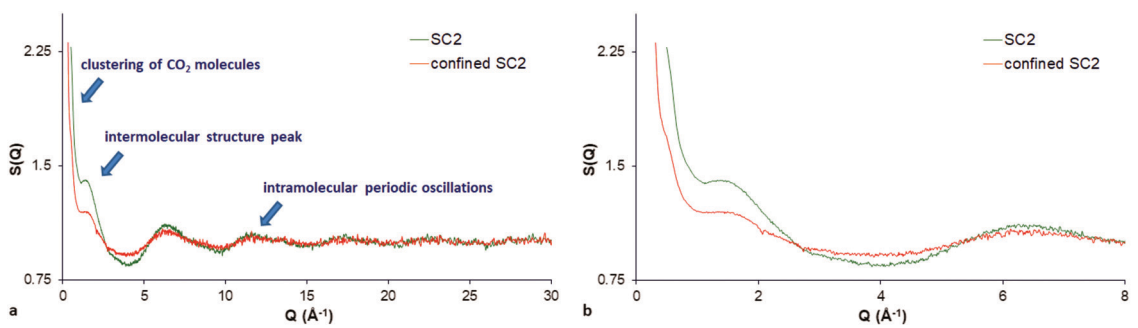

Fig. 2 The total scattering structure factor S(Q) for (a) bulk (SC2) and confined supercritical CO_2 (confined SC2) at 393 K and 180 bar respectively; (b) zoomed view of the low-Q region.

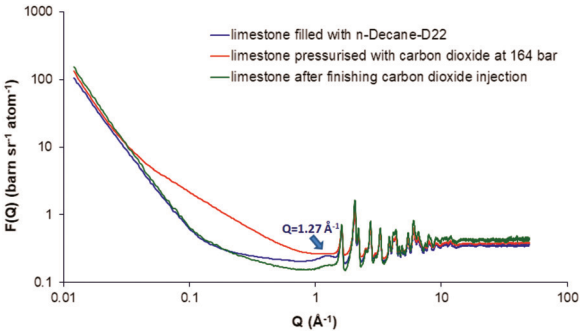

Fig. 3 Neutron scattering profiles of limestone sample filled with deuterated *n*-decane during (P = 164 bar) and after finishing the CO_2-EOR process at 393 K.

curve). However, there is still a remaining decane amount that was not displaced because a fraction of decane possibly entrapped over the limestone surfaces and through the pore throats. Another reason could be that the supercritical CO_2 pressure was close to the MMP value. This partial decane displacement is further supported by the intensity increase at low Q values followed by a decrease in intensity at high Qs (for more details, see ESI,† Section 5).

Fig. 4 illustrates schematically the CO_2-EOR process at the nanoscale based on the neutron scattering observations. Fig. 4a shows the pores of the reservoir matrix, *e.g.* limestone, partially filled with oil. The presence of a fraction of inaccessible (closed) pores can be also seen as calculated by the analysis of our neutron results. During CO_2 injection, the supercritical CO_2 dissolves causing the reservoir oil to swell (Fig. 4b and c). After the end of the process, a remarkable amount of oil has been recovered except of an amount possibly remained over the limestone surfaces and through the pore throats (Fig. 4d).

We therefore attempted to monitor the CO_2-EOR mode in real time at the nanoscale by combining total neutron scattering and SANS techniques. One major advantage of the technique is that the decane presence (or displacement) can be directly visualised by the appearance (or elimination) of the peak located at 1.27 $Å^{-1}$ followed by the intensity variations in the scattering curves throughout the whole Q range. In addition, the structural details of confined CO_2 can also be revealed and compared to those of CO_2 in bulk state (Section 3b and 2 ESI†). The most striking finding is that the clustering of CO_2 molecules still exists even when confined in the pores of the limestone. Finally, the pore accessibility to CO_2 has also been evaluated (Section 3a and 4 ESI†). The fact that only a small volume fraction of small mesopores is accessible to CO_2 will have implications for geologic CO_2 sequestration in limestone reservoirs.

As a result, a new methodology could be established for monitoring dynamically the CO_2-EOR process in real time at the nanoscale. As a future plan the potential of various additives could be further explored in order to provide valuable information both about their performance on the miscibility enhancement of the CO_2 and the oil and the lowering of the MMP. Furthermore, the structure of confined CO_2 in the presence of additives can be also proved to be crucial for their performance. For instance, the reduction of clustering of CO_2 molecules confined in the pores could be directly related to the improvement due to the additives performance. This feedback could also play an important role towards the development of additives to face existing issues of CO_2-EOR and, in general, on significantly improving our understanding of EOR approaches.

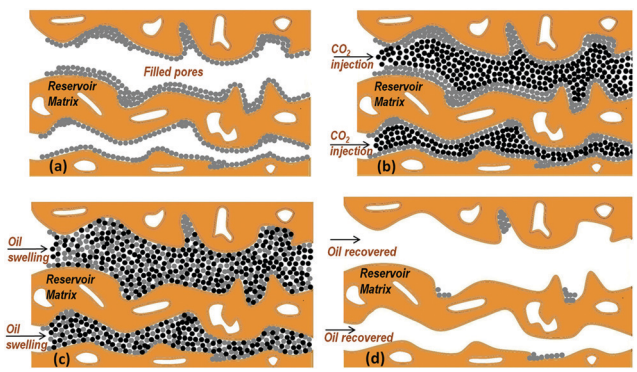

Fig. 4 Schematic of the CO_2-EOR process at the nanoscale based on the neutron scattering observations: (a) a reservoir matrix partially filled with oil; (b) injection of supercritical CO_2; (c) oil swelling; (d) oil recovery.

4. Summary and conclusions

In conclusion, a methodology has been established for monitoring the CO_2-EOR process in real time at the nanoscale. This was achieved by carrying out *in situ* neutron scattering measurements upon injection of supercritical CO_2 at a limestone sample loaded with deuterated *n*-decane. NIMROD was the ideal instrument for this study because it combines total neutron scattering and a significant part of SANS. The neutron results showed directly the decane recovery after the end of the supercritical CO_2 injection. This was achieved by observation of the decane peak and the intensity variations in the scattering curves. The results also suggested that there was still a remaining decane amount possibly entrapped over the matrix surfaces and through the pore throats. In addition, another important finding was that only a small fraction of the smaller mesopores is accessible to CO_2. This finding strongly suggests that this class of pores is unlikely sites for underground CO_2 sequestration. Furthermore, structural analysis revealed that the confined supercritical CO_2 is in a densified supercritical state with higher density compared to the bulk phase suggesting the physical ability of carbon dioxide molecules to pack perfectly within the pores of the limestone matrix. The most striking finding, however, is that that the clustering of supercritical CO_2 molecules also exists when confined within the limestone pores. From this point of view, a possible decrease in CO_2 clustering could be proved to be important for the additive performance to enhance oil recovery. To this end, a fruitful future research direction is under planning to apply the methodology in order to correlate the CO_2 structural properties in

the presence of additives with the recovery enhancement of the CO_2-EOR process.

Conflicts of interest

There are no conflicts to declare.

Acknowledgements

We gratefully acknowledge Khalifa University for the financial support through the CIRA-2019-002 project. Support by the Research and Innovation Center on CO_2 and H_2 (RICH, RC2-2019-007) of Khalifa University is also acknowledged. We are also grateful to the Science and Technology Facilities Council (STFC) for access to neutron beam time at NIMROD instrument (RB1920208) located at ISIS Neutron and Muon Source, Rutherford Appleton Laboratory, Oxfordshire, United Kingdom.

Notes and references

1 O. Massarweh and A. S. Abushaikha, A review of recent developments in CO_2 mobility control in enhanced oil recovery, *Petroleum*, 2022, DOI: 10.1016/j.petlm.2021.05.002.
2 J. S. Levine, I. Fukai, D. J. Soeder, G. Bromhal, R. M. Dilmore, G. D. Guthrie, T. Rodosta, S. Sanguinito, S. Frailey, C. Gorecki, W. Peck and A. L. Goodman, U.S. DOE NETL methodology for estimating the prospective CO_2 storage resource of shales at the national and regional scale, *Int. J. Greenhouse Gas Contr.*, 2016, **51**, 81–94.
3 K. N. Mavar, N. Gaurina-Međimurec and L. Hrnčević, Significance of Enhanced Oil Recovery in Carbon Dioxide Emission Reduction, *Sustainability*, 2021, **13**, 1800.
4 C. Hepburn, E. Adlen, J. Beddington, E. A. Carter, S. Fuss, N. Mac Dowell, J. C. Minx, P. Smith and C. K. Williams, The technological and economic prospects for CO_2 utilization and removal, *Nature*, 2019, **575**, 87–97.
5 C. Kolster, M. S. Masnadi, S. Krevor, N. Mac Dowell and A. R. Brandt, CO_2 enhanced oil recovery: a catalyst for gigatonne-scale carbon capture and storage deployment?, *Energy Environ. Sci.*, 2017, **10**, 2594–2608.
6 M. Bui, C. S. Adjiman, A. Bardow, E. J. Anthony, A. Boston, S. Brown, P. S. Fennell, S. Fuss, A. Galindo, L. A. Hackett, J. P. Hallett, H. J. Herzog, G. Jackson, J. Kemper, S. Krevor, G. C. Maitland, M. Matuszewski, I. S. Metcalfe, C. Petit, G. Puxty, J. Reimer, D. M. Reiner, E. S. Rubin, S. A. Scott, N. Shah, B. Smit, J. P. M. Trusler, P. Webley, J. Wilcoxx and N. Mac Dowell, Carbon capture and storage (CCS): the way forward, *Energy Environ. Sci.*, 2018, **11**, 1062–1176.
7 N. Mac Dowell, P. S. Fennell, N. Shah and G. C. Maitland, The role of CO_2 capture and utilization in mitigating climate change, *Nat. Clim. Change*, 2017, **7**, 243–249.
8 W. Jia, B. McPherson, F. Pan, Z. Dai, N. Moodie and T. Xiao, Impact of Three-Phase Relative Permeability and Hysteresis Models on Forecasts of Storage Associated With CO_2-EOR, *Water Resour. Res.*, 2018, **54**, 1109–1126.
9 Z. Dai, R. Middleton, H. Viswanathan, J. Fessenden-Rahn, J. Bauman, R. Pawar, S.-Y. Lee and B. McPherson, An Integrated Framework for Optimizing CO_2 Sequestration and Enhanced Oil Recovery, *Environ. Sci. Technol. Lett.*, 2014, **1**, 49–54.
10 W. Ampomaha, R. S. Balch, M. Cather, R. Will, D. Gunda, Z. Dai and M. R. Soltanian, Optimum design of CO_2 storage and oil recovery under geological uncertainty, *Appl. Energy*, 2017, **195**, 80–92.
11 Z. Dai, H. Viswanathan, R. Middleton, F. Pan, W. Ampomah, C. Yang, W. Jia, T. Xiao, S.-Y. Lee, B. McPherson, R. Balch, R. Grigg and M. White, An Integrated Framework for Optimizing CO_2 Sequestration and Enhanced Oil Recovery, *Environ. Sci. Technol.*, 2016, **50**, 7546–7554.
12 Q. Lyu, J. Tan, L. Li, Y. Ju, A. Busch, D. A. Wood, P. G. Ranjith, R. Middleton, B. Shu, C. Hu, Z. Wanga and R. Hua, The role of supercritical carbon dioxide for recovery of shale gas and sequestration in gas shale reservoirs, *Energy Environ. Sci.*, 2021, **14**, 4203–4227.
13 F. M. Orr and J. J. Taber, Use of Carbon Dioxide in Enhanced Oil Recovery, *Science*, 1984, **224**, 563–569.
14 M. K. Verma, *Fundamentals of carbon dioxide-enhanced oil recovery (CO_2-EOR)-A supporting document of the assessment methodology for hydrocarbon recovery using CO_2-EOR associated with carbon sequestration*, U.S. Geological Survey Open-File Report, 2015, **1071**, 19p.
15 S. F. Janna and F. Le-Hussain, Effectiveness of modified CO_2 injection at improving oil recovery and CO_2 storage—Review and simulations, *Energy Rep.*, 2020, **6**, 1922–1941.
16 G. A. Mansoori and S. A. Rice, Confined Fluids: Structure, Properties and Phase Behavior, in *Advances in Chemical Physics*, ed. S. A. Rice and A. R. Dinner, John Wiley & Sons, 2015, vol. 156, pp. 197–294.
17 F.-X. Coudert, A. Boutin and A. H. Fuchs, Open questions on water confined in nanoporous materials, *Commun. Chem.*, 2021, **4**, 106.
18 J. D. F. Ramsay, Surface and pore structure characterisation by neutron scattering techniques, *Adv. Colloid Interface Sci.*, 1998, **76-77**, 13–37.
19 Y. B. Melnichenko, *Small-angle scattering from confined and interfacial fluids: Applications to energy storage and environmental science*, Springer, 2015.
20 M. C. Schlegel, V. Grzimek, G. Günther, R. Svetogorov, C. M. Veziri, M. Kapsi, G. N. Karanikolos, O. Prokhnenko, R. Bewley and M. Russina, Explaining water adsorption in one-dimensional channels in AlPO4-5 on molecular scale, *Microporous Mesoporous Mater.*, 2020, **304**, 109201.
21 M. Russina, G. Günther, V. Grzimek, M. C. Schlegel, C. M. Veziri, G. N. Karanikolos, T. Yamada and F. Mezei, Nanoscale Dynamics and Transport in Highly Ordered Low-Dimensional Water, *J. Phys. Chem. Lett.*, 2019, **10**, 6339–6344.
22 Y. Ren and X. Zuo, Synchrotron X-Ray and Neutron Diffraction, Total Scattering, and Small-Angle Scattering Techniques for Rechargeable Battery Research, *Small Methods*, 2018, **2**, 1800064.

23 D. T. Bowron, A. K. Soper, K. Jones, S. Ansell, S. Birch, J. Norris, L. Perrott, E. D. Riedel, N. J. Rhodes, S. R. Wakefield, A. Botti, M.-A. Ricci, F. Grazzi and M. Zoppi, NIMROD: The Near and InterMediate Range Order Diffractometer of the ISIS second target station, *Rev. Sci. Instrum.*, 2010, **81**, 033905.

24 T. A. Steriotis, K. L. Stefanopoulos, F. K. Katsaros, R. Gläser, A. C. Hannon and J. D. F. Ramsay, In situ neutron diffraction study of adsorbed carbon dioxide in a nanoporous material: monitoring the adsorption mechanism and the structural characteristics of the confined phase, *Phys. Rev. B: Condens. Matter Mater. Phys.*, 2008, **78**, 115424.

25 K. L. Stefanopoulos, T. A. Steriotis, F. K. Katsaros, N. K. Kanellopoulos, A. C. Hannon and J. D. F. Ramsay, Structural study of supercritical carbon dioxide confined in nanoporous silica by in situ neutron diffraction, *J. Phys.: Conf. Ser.*, 2012, **340**, 012049.

26 K. L. Stefanopoulos, F. K. Katsaros, Th. A. Steriotis, A. A. Sapalidis, M. Thommes, D. T. Bowron and T. G. A. Youngs, Anomalous depletion of pore-confined carbon dioxide upon cooling below the bulk triple point: an in situ neutron diffraction study, *Phys. Rev. Lett.*, 2016, **116**, 025502.

27 K. L. Stefanopoulos, C. Tampaxis, A. A. Sapalidis, F. K. Katsaros, T. G. A. Youngs, D. T. Bowron and T. A. Steriotis, Total neutron scattering study of supercooled CO_2 confined in an ordered mesoporous carbon, *Carbon*, 2020, **167**, 296–306.

28 A. K. Soper and D. T. Bowron, Density profile of nitrogen in cylindrical pores of MCM-41, *Chem. Phys. Lett.*, 2017, **683**, 529–535.

29 M. Falkowska, D. T. Bowron, H. Manyar, T. G. A. Youngs and C. Hardacre, Confinement effects on the benzene orientational structure, *Angew. Chem.*, 2018, **130**, 1–7.

30 K. L. Stefanopoulos, T. G. A. Youngs, R. Sakurovs, L. F. Ruppert, J. Bahadur and Y. B. Melnichenko, Neutron Scattering Measurements of Carbon Dioxide Adsorption in Pores within the Marcellus Shale: Implications for Sequestration, *Environ. Sci. Technol.*, 2017, **51**, 6515–6521.

31 L. F. Ruppert, A. M. Jubb, T. F. Headen, T. G. A. Youngs and B. Bandli, Impacts of Mineralogical Variation on CO_2 Behavior in Small Pores from Producing Intervals of the Marcellus Shale: Results from Neutron Scattering, *Energy Fuels*, 2020, **34**, 2765–2771.

32 F. K. Katsaros, T. A. Steriotis, K. L. Stefanopoulos, N. K. Kanellopoulos, A. C. Mitropoulos, M. Meissner and A. Hoser, Neutron diffraction study of adsorbed CO_2 on a carbon membrane, *Phys. B*, 2000, **276–278**, 901–902.

33 T. A. Steriotis, K. L. Stefanopoulos, A. C. Mitropoulos, N. K. Kanellopoulos, A. Hoser and M. Hofmann, Structural Studies of Supercritical CO_2 in Confined Space, *Appl. Phys. A: Mater. Sci. Process*, 2002, **74**, s1333–s1335.

34 T. A. Steriotis, K. L. Stefanopoulos, N. K. Kanellopoulos, A. C. Mitropoulos and A. Hoser, The structure of adsorbed CO_2 in carbon nanopores; a neutron diffraction study, *Colloids Surf., A*, 2004, **241**, 239–244.

35 J. Bahadur, Y. B. Melnichenko, L. He, C. I. Contescu, N. C. Gallego and J. R. Carmichael, SANS investigations of CO_2 adsorption in microporous carbon, *Carbon*, 2015, **95**, 535–544.

36 A. P. Radlinski, Small-Angle Neutron Scattering and the Microstructure of Rocks, *Rev. Mineral. Geochem.*, 2006, **63**, 363–397.

37 T. E. Mares, A. P. Radliński, T. A. Moore, D. Cookson, P. Thiyagarajan, J. Ilavsky and J. Klepp, Location and Distribution of Inorganic Material in a Low Ash Yield, Subbituminous Coal, *Int. J. Coal Geol.*, 2012, **94**, 173–181.

38 A. P. Radlinski and M. Mastalerz, Neutron Scattering Study of Vitrinite: Insights into Sub-Micrometer Inclusions in North American Carboniferous Coals of Bituminous Rank, *Int. J. Coal Geol.*, 2018, **186**, 145–154.

39 K. L. Stefanopoulos, G. E. Romanos, A. C. Mitropoulos, N. K. Kanellopoulos and R. K. Heenan, Characterisation of porous alumina membrane by adsorption in conjunction with SANS, *J. Membr. Sci.*, 1999, **153**, 1–7.

40 The reason is that H and D have neutron scattering lengths of opposite sign; this means that by filling the pores using an appropriate mixture of hydrogenous and deuterated solvents (such as H_2O/D_2O) the neutron scattering length density of the porous solid becomes equal to that of the liquid mixture and contrast matching is achieved.

41 P. J. Hall, S. D. Brown and J. M. Calo, The pore structure of the Argonne coals as interpreted from contrast matching small angle neutron scattering, *Fuel*, 2000, **79**, 1327–1332.

42 K. Mergia, K. L. Stefanopoulos, N. Ordás and C. García-Rosales, A comparative study for the porosity of doped graphites by small angle neutron scattering, nitrogen adsorption and helium pycnometry, *Microporous Mesoporous Mater.*, 2010, **134**, 141–149.

43 X. Gu, D. F. R. Mildner, D. R. Cole, G. Rother, R. Slingerland and S. L. Brantley, Quantification of Organic Porosity and Water Accessibility in Marcellus Shale Using Neutron Scattering, *Energy Fuels*, 2016, **30**, 4438–4449.

44 J. Bahadur, L. F. Ruppert, V. Pipich, R. Sakurovs and Y. B. Melnichenko, Porosity of the Marcellus Shale: A Contrast Matching Small-Angle Neutron Scattering Study, *Int. J. Coal Geol.*, 2018, **188**, 156–164.

45 R. Sakurovs, L. Koval, M. Grigore, A. Sokolova, L. de Campo and C. Rehm, Nanostructure of Cokes, *Int. J. Coal Geol.*, 2018, **188**, 112–120.

46 G. Sang, S. Liu, D. Elsworth, R. Zhang and M. Bleuel, Pore-Scale Water Vapor Condensation Behaviors in Shales: An Experimental Study, *Transport Porous Media*, 2020, **135**, 713–734.

47 J. Bahadur, C. R. Medina, L. He, Y. B. Melnichenko, J. A. Rupp, T. P. Blach and D. F. R. Mildner, Determination of closed porosity in rocks by small-angle neutron scattering, *J. Appl. Crystallogr.*, 2016, **49**, 2021–2030.

48 Y. B. Melnichenko, L. He, R. Sakurovs, A. L. Kholodenko, T. Blach, M. Mastalerz, A. P. Radlinski, G. Cheng and D. F. R. Mildner, Accessibility of Pores in Coal to Methane and Carbon Dioxide, *Fuel*, 2012, **91**, 200–208.

49 R. Sakurovs, L. He, Y. B. Melnichenko, A. P. Radlinski, T. Blach, H. Lemmel and D. F. R. Mildner, Pore Size Distribution and Accessible Pore Size Distribution in Bituminous Coals, *Int. J. Coal Geol.*, 2012, **100**, 51–64.

50 L. He, Y. B. Melnichenko, M. Mastalerz, R. Sakurovs, A. P. Radlinski and T. Blach, Pore Accessibility by Methane and Carbon Dioxide in Coal as Determined by Neutron Scattering, *Energy Fuels*, 2012, **26**, 1975–1983.

51 R. Zhang, S. Liu, J. Bahadur, D. Elsworth, Y. Melnichenko, L. He and Y. Wang, Estimation and modeling of coal pore accessibility using small angle neutron scattering, *Fuel*, 2015, **161**, 323–332.

52 M. Mastalerz, L. He, Y. B. Melnichenko and J. A. Rupp, Porosity of Coal and Shale: Insights from Gas Adsorption and SANS/USANS Techniques, *Energy Fuels*, 2012, **26**, 5109–5120.

53 L. F. Ruppert, R. Sakurovs, T. P. Blach, L. He, Y. B. Melnichenko, D. F. R. Mildner and L. Alcantar-Lopez, A USANS/SANS Study of the Accessibility of Pores in the Barnett Shale to Methane and Water, *Energy Fuels*, 2013, **27**, 772–779.

54 C. R. Clarkson, N. Solano, R. M. Bustin, A. M. M. Bustin, G. R. L. Chalmers, L. He, Y. B. Melnichenko, A. P. Radlinski and T. P. Blach, Pore Structure Characterization of North American Shale Gas Reservoirs Using USANS/SANS, Gas Adsorption, and Mercury Intrusion, *Fuel*, 2013, **103**, 606–613.

55 D. T. Bowron and A. K. Soper, Taking Atomistic Insight into the Nanoscale: Nimrod, the Near and Intermediate Range order Diffractometer, *Neutron News*, 2011, **22**, 12–14.

56 A. K. Soper, GudrunN and GudrunX Programs for Correcting Raw Neutron and X-Ray Total Scattering Data to Differential Cross Section, https://www.isis.stfc.ac.uk, 2012.

57 A. P. Radliński, C. J. Boreham, P. Lindner, O. Randl, G. D. Wignall, A. Hinde and J. M. Hope, Small angle neutron scattering signature of oil generation in artificially and naturally mature hydrocarbon source rocks, *Org. Geochem.*, 2000, **31**, 1–14.

58 C. Alba-Simionesco, G. Dosseh, E. Dumont, B. Frick, B. Geil, D. Morineau, V. Teboul and Y. Xia, Confinement of molecular liquids: consequences on thermodynamic, static and dynamical properties of benzene and toluene, *Eur. Phys. J. E: Soft Matter Biol. Phys.*, 2003, **12**, 19–28.